Contents

Chapter 1

Cyclotron

In addition to introducing to the cyclotron accelerator this first chapter starts bringing in beam optics notions and notations which will be manipulated throughout the course (orbit, index, wedge angle, periodicity, periodic stability, tunes, momentum compaction, dispersion function, etc.). It also familiarizes with ray-tracing and computer program simulations, starting with short, simple, optical sequences.

1.1 Introduction

The cyclotron arrived at a time, $\sim$1930, where techniques to accelerate ions were sought, for the study of nuclear properties of the atom. To this day, hundreds of cyclotrons have been built, and more still are, to accelerate protons, ions, radioactive isotopes. They are used in domains as varied as particle factories (muons, neutrons), protontherapy, production of radio-isotopes for medicine, etc.

The cyclotron was conceived as a means to overcome the inconvenient of using a long series of high electric field electrodes in a linear layout, by repeated recirculation of the particles across an electric gap formed by a pair of cylindrical electrodes. The recirculation is obtained by plunging the electrodes in a uniform magnetic field which causes the ions to undergo, as they are accelerated, a spiraling motion with increasing radius, confined in the vicinity of a plane normal to the field (Fig. 1.3). A fixed frequency oscillating voltage is applied to the electrodes. While an accelerated bunch spirals outward, the increase in the distance it travels over a turn is compensated by its velocity increase, so that, in the non-relativistic approximation ($\gamma \approx 1$), the revolution time $\mathrm{T_{rev}}$ remains constant; with the appropriate voltage frequency $\mathrm{f_{RF}} \approx \mathrm{h/T_{rev}}$ the revolution can be maintained in close

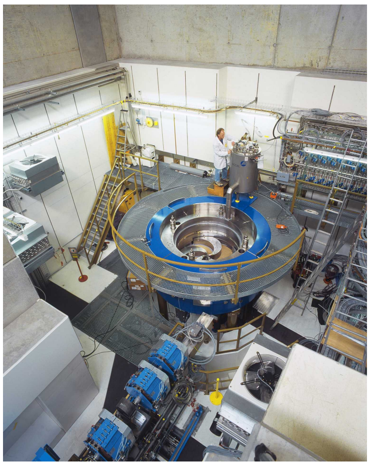

Fig. 1.1 Superconducting-coil isochronous spiral-sector AVF cyclotron at PSI, providing 250 MeV, 500 nA beams for hadrontherapy.

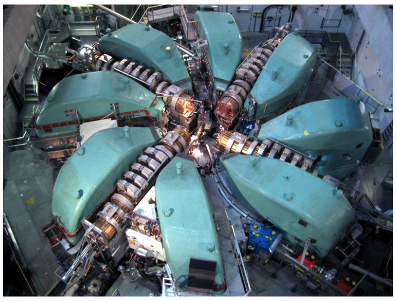

Fig. 1.2 PSI high power cyclotron. It delivers a 590 MeV, 1.4 MW, CW proton beam for secondary particle production (*e.g.*, neutron, muon).

synchronism with the RF wave, Trev $\approx$ hT_{RF}, so that the bunch transit the accelerating gap during the accelerating phase of V(t) (Fig. 1.4).

• Exercise 1.1-1. The optical sequence for this exercise is given in appendix 1.5.1. Let's check that the revolution time is constant, independent of particle velocity. Construct a 360-degree mid-plane 2-dimensional field map, using a uniform mesh in cylindrical coordinates covering R=10 to 70 cm, with constant axial field B=0.5 T. Launch particles with normalized velocity $\beta = v/c \ll 1$ (equivalently, Lorentz relativistic factor $\gamma = 1/\sqrt{1-\beta^2} \approx 1$), plot the revolution time as a function of velocity. •

Principle

In the uniform axial field B a particle with relativistic mass $m = \gamma m_0$, charge q, momentum p = mv, undergoes a circular motion characterized by its radius R, with a revolution period T_{rev} which depends on the field and on the particle charge and mass, but *not* on R neither on particle velocity.

• Exercise 1.1-2. While we are here, let's see what our code tells about the energy dependence of velocity and mass of a particle:
(a) Take an optical sequence which is just an accelerating gap, with peak voltage, say, 100 kV. Inject a proton with starting kinetic energy, say,

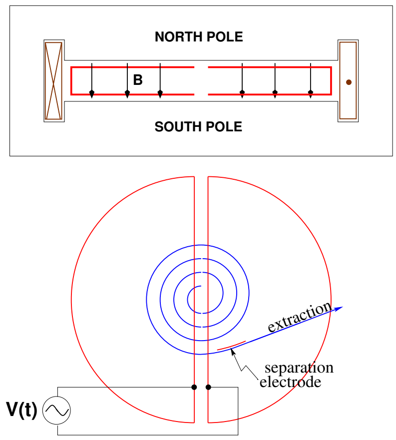

Fig. 1.3 Cyclotron : trajectories spiral in the uniform magnetic field between two circular poles. A double-dee forms a gap which is applied an oscillating voltage V(t) with frequency an integer multiple h of the revolution frequency, causing particles with the proper phase with respect to V(t) to be accelerated.

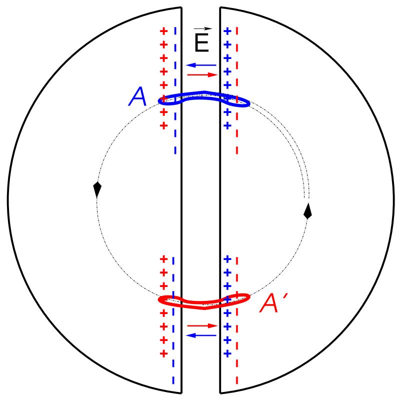

Fig. 1.4 Resonant acceleration: a bunch meeting an accelerating field $\tilde{\mathrm{E}}$ across the gap at A, at time t, will meet again, half a revolution later, at time $\mathrm{t}+\mathrm{T_{rev}}/2=\mathrm{t}+\mathrm{hT_{RF}}/2$, an accelerating field $\tilde{\mathrm{E}}$ across the gap at A', and so forth.

In passing: check the consistency of the coil current, direction of $\vec{B}$ and particle rotation - what is the sign of the accelerated particles?

20 keV, let it go repeatedly through the gap until it reaches 3 GeV kinetic energy about. Plot its momentum pc and total energy E as a function of its kinetic energy, both from this numerical experiment and from theory, everything on the same graph, use MeV units.
(b) Plot the theoretical normalized velocity $\beta = \mathrm{v/c}$, both actual and in the case of the classical approximation $\gamma = 1$. Plot the numerical value obtained from ray-tracing. All on the same graph. •

It is not possible to accelerate a particle traveling on a closed path using an electrostatic field $\tilde{\mathrm{E}} = -\tilde{\mathrm{grad}}\mathrm{V}(\tilde{\mathrm{R}},\mathrm{t})$ as the work by $\tilde{\mathrm{F}} = \mathrm{q}\tilde{\mathrm{E}}$ only depends on the initial and final states, it is independent of the path (Fig. 1.5):

$$\mathrm{W} = \int_\mathrm{A}^\mathrm{B} \tilde{\mathrm{F}}.\mathrm{d}\tilde{\mathrm{s}} = -\mathrm{q}\int_\mathrm{A}^\mathrm{B} \tilde{\mathrm{grad}}\mathrm{V}.\mathrm{d}\tilde{\mathrm{s}} = -\mathrm{q}(\mathrm{V_B}-\mathrm{V_A}).$$
$$\text{On a closed path}: \oint \tilde{\mathrm{F}}.\mathrm{d}\tilde{\mathrm{s}} = 0 \tag{1.1}$$

Instead, the work of a force of induction origin (the electric field arises from the variation of a magnetic flux, $\vec{E} = -\partial\vec{A}/\partial t$, $\tilde{\mathrm{A}}$ a vector potential) may not be null on a closed path. This is achieved *for instance* using

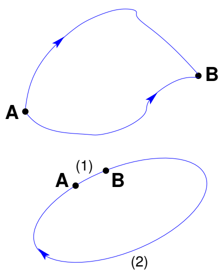

Fig. 1.5 The work of the electrostatic force only depends on V_A and V_B, independent of the path. In the case of the closed path: the particle loses along (2) the energy gained along (1).

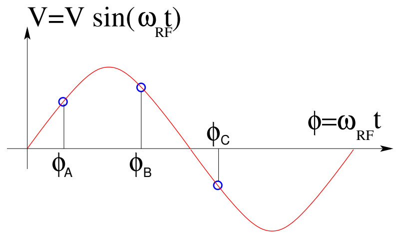

Fig. 1.6 A particle which reaches the gap at $\omega_{\rm RF}{\rm t} = \phi_{\rm A}$ or $\omega_{RF}t = \phi_B$ is accelerated, at $\omega_{\rm RF}{\rm t} = \phi_{\rm C}$ it is decelerated.

a radio-frequency system which feeds an oscillating voltage across a gap, $\hat{\rm V}\sin(2\pi {\rm f_{RF}t} + \phi)$ (Fig. 1.6). In the classical cyclotron the gap is formed mechanically by a double dee system (Fig. 1.3), The quantities of concern, regarding orbital motion (R, $\rm f_{rev} = \omega_{rev}/2\pi$), field (B), voltage ($\hat{\rm V}$, $f_{\rm RF} = \omega_{RF}/2\pi$), satisfy

$$\rm BR = p/q, \qquad 2\pi f_{rev} = v/R = qB/m, \qquad f_{RF} = hf_{rev} \tag{1.2}$$

The two frequencies are in the harmonic ratio h. These relationships hold whatever γ, from $v \ll c$ ($\gamma \approx 1$, domain of the *classical* cyclotron technology) to $\gamma > 1$ (domain of the *isochronous* cyclotron technology).

Note the first quantity introduced above, the *rigidity* of the particle of charge q and momentum p, $BR = p/q$ (often noted $B\rho = p/q$ as well), with R (or ρ) the curvature radius of the trajectory under the effect of the Laplace force in the field B. This is a quantity of predilection in accelerator physics and design, it will be omnipresent along these lectures.

The energy gain, or loss, by the particle when transiting the gap is

$$\Delta {\rm W} = {\rm q}\hat{\rm V}\sin\phi \quad \text{with } \phi = \omega_{\rm RF}{\rm t} - \omega_{\rm rev}{\rm t} + \phi_0 \tag{1.3}$$

with ϕ its phase with respect to the RF signal at the gap (*e.g.*, $\phi_{\rm A}$, $\phi_{\rm B}$ or ϕ_C in Fig. 1.6) and ϕ_0 the value at $t = 0$, $\omega_{\rm rev}{\rm t}$ the orbital angle of the particle.

• Exercise 1.1-3. Explain what happens if a single RF gap is used. Simulate that in the following way:

1.1-3.a - Build an optical sequence using the field map fabricated in exercise 1.1-1. Install an accelerating gap downstream of the field map. Launch a

200 keV proton on a starting R=12.9248888074 cm. Track over a few passes and plot the trajectory in the field map.

1.1-3.b - Now, split the field map into two 180 degree halves and add a second gap opposing in diameter. Accelerate in a similar way: assuming the same constant kick at each gap. Plot the spiraling trajectory, superimpose the expected theoretical spiral. •

1.2 Classical cyclotron

Fixed-frequency acceleration requires matching between the RF and cyclotron frequencies. However the relativistic increase of the mass causes the revolution period to decrease with momentum, $\Delta\mathrm{T_{rev}}/\mathrm{T_{rev}} = \gamma - 1$.

• Exercise. Demonstrate that relationship. •

The mis-match between the accelerating and cyclotron frequencies is a turn-by-turn cumulative effect and sets a limit to the highest velocity, $\beta = \mathrm{v/c} \approx 0.22$, $\Delta\mathrm{T_{rev}}/\mathrm{T_{rev}} \approx 2-3\%$. This means for instance a limit of applicability of the "classical cyclotron" in the region $\mathrm{E} - \mathrm{mc}^2 \lesssim 25$ MeV for protons, $\lesssim 50$ MeV for D and α particles.

1.2.1 *Fixed-energy orbits, revolution period*

A common method for realistic modeling of the magnetic field of a cyclotron is to use a field map. Using a mathematical model is also a reasonable approach in a preliminary design phase due to the flexibility it brings in possibly tweaking parameters as for instance field homogeneity, or its radial or azimuthal dependence. These two techniques are employed in the exercises to come.

• Exercise 1.2.1-1.

1.2.1-1.a - Split into six 60 degree sectors the field map constructed in Ex. 1.1. Plot, as a function of energy, the radius R and revolution period $\mathrm{T_{rev}}$ for closed orbits at fixed energy, from both ray-tracing and simple geometry, on a the same graphic for comparison. Explain what causes the slow increase of revolution period with energy.

1.2.1-1.b - Check the evolution of orbit radius and revolution period with field map mesh density: re-compute the 60 degree sector field map with various mesh sizes. Similarly: check the effect of the integration step size on these quantities.

1.2.1-1.c - Use instead a theoretical modeling for the field and re-do the exercise above (the optical sequence for this exercise is given in appendix **??**).

From the two series of results, comment on various pros and cons of the two methods, analytical field models and field maps. •

• Exercise 1.2.1-2: cyclotron extraction and limitation in energy. It follows from $\mathrm{qBR} = \mathrm{p} = \sqrt{2\mathrm{mW}}$ (in the classical approximation, and with W the kinetic energy) that $\frac{\Delta \mathrm{R}}{\mathrm{R}} = \frac{1}{2}\frac{\Delta \mathrm{W}}{\mathrm{W}}$. with ΔW the (constant) energy gain per turn, this yields $\mathrm{dR} = \frac{\mathrm{m}\Delta\mathrm{W}}{\mathrm{q}^2\mathrm{B}^2\mathrm{R}}$: the radius increment ΔR decreases with R. As the extraction at the last turn requires sufficient separation from the last but one, for insertion of a deflector electrode, there is a feasibility limit. Plot the accelerated spiral, or the fixed-energy orbits, to top energy, observe this property. Plot $dR(R)$, from both tracking and theory. •

Periodic motion - Horizontal motion in a uniform field cyclotron has no privileged reference orbit: for a given momentum, the initial radius and velocity vector define a particular closed, circular orbit. A particle launched with an axial velocity component on the other hand, drifts vertically linearly with time, as there is no axial restoring strength component. The next Section will investigate the necessary field property, absent in our present field model, proper to ensure confinement of the multiturn periodic motion in the vicinity of the median plane of the cyclotron dipole magnet.

• Exercise 1.2.1-3. Observe the first statement above by plotting trajectories of particles launched with different initial velocity vector (zero axial component) over one turn. Observe the second statement by plotting the axial coordinate of a particle launched with an axial initial velocity component. •

1.2.2 *Weak focusing*

Let $\mathrm{B_r(r)}$, $\mathrm{B_y(r)}$ be respectively the radial and axial components of the magnetic field at a small radial displacement $(\mathrm{x} = \mathrm{r} - \mathrm{R}, \mathrm{y})$ from the reference circular orbit at R (centered at the center of the axially symmetric cyclotron magnet, Fig. 1.7). And by median-plane symmetry of the field, $\mathrm{B_r}|_{\mathrm{y}=0} = 0$ at all r (Fig. 1.7). The radial and axial forces experienced by a particle at r, where the curvature radius is $r = R + x$, write, to the first order in the radial and axial coordinates, respectively x and y,

$$\mathrm{F_x} = \mathrm{m}\ddot{\mathrm{x}} = -\mathrm{qvB_y(r)} + \mathrm{m}\frac{\mathrm{v}^2}{\mathrm{R}+\mathrm{x}} \approx -\mathrm{qv}(\mathrm{B_y}|_{\mathrm{R}} + \left.\frac{\partial \mathrm{B_y}}{\partial \mathrm{r}}\right|_{\mathrm{R}}\mathrm{x}) + \mathrm{m}\frac{\mathrm{v}^2}{\mathrm{R}}(1-\frac{\mathrm{x}}{\mathrm{R}})$$

$$\mathrm{F_y} = \mathrm{m}\ddot{\mathrm{y}} = \mathrm{qvB_r(r)} = \mathrm{qv}\left.\frac{\partial \mathrm{B_r}}{\partial \mathrm{y}}\right|_{\mathrm{y}=0}\mathrm{y} + \text{higher order} \approx \mathrm{qv}\frac{\partial \mathrm{B_y}}{\partial \mathrm{r}}\mathrm{y} \qquad (1.4)$$

Note that the force F_x which applies on the ions is the resultant of the pseudo force $f_c = m\frac{v^2}{R}$, oriented away from the center of the motion, and of the magnetic force $f_B = -qvB_y(r)$, oriented toward the center of the motion. In particular, $-qvB_y|_R + m\frac{v^2}{R} = 0$. These relations yield the differential equations for the radial and axial motions, respectively,

$$\ddot{x} + \omega_r^2 x = 0 \qquad \text{and} \qquad \ddot{y} - \omega_y^2 y = 0 \tag{1.5}$$

wherein $\omega_r^2 = \omega_{rev}^2(1 + \frac{R}{B}\frac{\partial B_y}{\partial r})$, $\omega_y^2 = \omega_{rev}^2 \frac{R}{B}\frac{\partial B_y}{\partial r}$, with $\omega_{rev} = 2\pi f_{rev}$ the angular frequency of the circular motion. Focusing by a restoring force appears (Eq. 1.5) owing to the use of a magnetic field with radial index

$$k(R) = \frac{R}{B}\frac{\partial B_y}{\partial r}|_{r=R,y=0} \tag{1.6}$$

Radial stability in an axially symmetric structure with weakly decreasing field B(r) is sketched in Fig. 1.7-left : At larger motion radius, $r > R$ (resp. smaller, $r < R$), a particle with momentum $p = mv$ (assumed positively charged) experiences a decrease (resp. increase) of the outward force $f_c = m\frac{v^2}{R}$ ($R = p/qB$ increases with r) at a higher rate than the decrease (resp. increase) of the bending force $f_B = -qvB$. In other words, radial stability requires BR to be an increasing function of R, $\frac{\partial BR}{\partial R} = B + R\frac{\partial B}{\partial R} > 0$ or $1 + k > 0$.

Axial stability imposes a guiding field decreasing with radius, Fig. 1.7-right, *i.e.*, $k < 0$. This ensures a restoring force directed toward the median plane.

The resulting condition of motion stability around the equilibrium orbit

$$-1 < k < 0 \tag{1.7}$$

is known as "weak focusing".

The two quantities

$$\nu_r = \omega_r/\omega_{rev} = \sqrt{1+k}, \qquad \nu_y = \omega_y/\omega_{rev} = \sqrt{-k} \tag{1.8}$$

are known as, respectively, the radial and axial "wave number" of the oscillatory motion around the reference circular orbit of radius R.

Field profile - Keeping the focusing constant (k = Const.) throughout the radial beam excursion requires an hyperbolic field profile: from Eq. 1.9 (and noting $B \equiv B_y$, assuming B only changes radially, introducing B_0: the field value at some reference radius r_0),

$$k = \frac{R}{B}\frac{dB}{dR} \Rightarrow \ln\frac{dB}{B} = k\ln\frac{dR}{R} \Rightarrow \frac{B}{B_0} = \left(\frac{R}{R_0}\right)^k \text{ or } B = B_0\left(\frac{R}{R_0}\right)^k \tag{1.9}$$

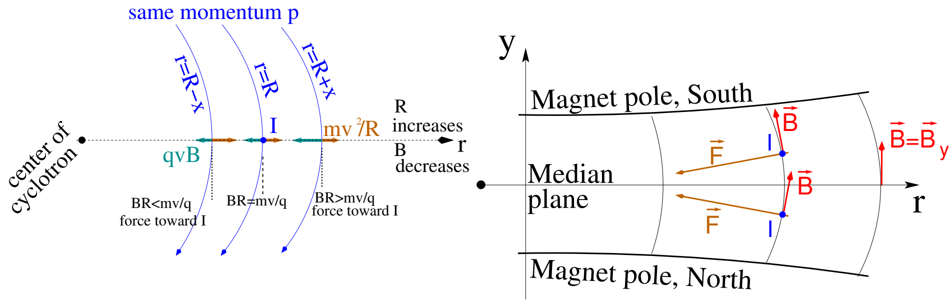

Fig. 1.7 Motion stability in a weak focusing axially symmetric structure. Left, radial: the resultant of the bending and outward forces pulls particles with momentum p = mv toward the equilibrium orbit at ρ = p/qB, resulting in a stable oscillation around the latter. Right, axial: positive ions off the median plane (at I, coming out of the page) experience a force pulling toward the median plane.

and B has to decrease with R to ensure vertical focusing, so $k < 0$.

• Exercise 1.2.2-1. Plot two particle trajectories that demonstrate the value of the radial wave number in a uniform field. Conclude on orbit and horizontal motion stability. Derive the horizontal and axial transport matrices from ray-tracing, conclude on the stability of the motion in a uniform field. •

• Exercise 1.2.2-2. Using the field map method of exercise 1.2.1-1 or the analytical modeling of exercise 1.2.1-2, introduce a radial field index $-1 < k < 0$ in the sector field. Plot the radial and axial paraxial motions of a 3 MeV ion over a few turns.
Plot the energy dependence of the reference orbit radius, R(E).
Plot the R-dependence of the revolution period T_{rev} for the magnet with field index, from both ray-tracing and theory. •

• Exercise 1.2.2-3. Using either the field map or the analytical model of exercise 1.2.2-2, compute its radial and axial motion wave numbers, ν_r and ν_y, using two different methods, namely, 1-turn mapping and Fourier analysis. Show that $\nu_r^2 + \nu_y^2 = 1$, at all radii. •

Isochronism - The focusing condition $-1 < k < 0$ breaks the isochronism as it causes the guiding field B and thus $\omega_{rev} = qB/m$ to change (decrease) with R. As a consequence, the arrival time of a particle at the RF gap (by extension the "RF phase" of the motion) is not constant.

1.2.3 *Coordinate transport*

Introducing time as the independent variable in Eq. 1.5, using the approximation ds ≈ vdt (and introducing a reference curvature radius ρ_0, and a different notation, n, for the field index, with $0 < \mathrm{n} < 1$), yields

$$\frac{\mathrm{d}^2\mathrm{x}}{\mathrm{ds}^2} + \frac{1-\mathrm{n}}{\rho_0^2}\mathrm{x} = 0, \qquad \frac{\mathrm{d}^2\mathrm{y}}{\mathrm{ds}^2} + \frac{\mathrm{n}}{\rho_0^2}\mathrm{y} = 0 \tag{1.10}$$

The solution to the motion writes

$$\begin{aligned} \mathrm{x(s)} =& \mathrm{x}_0 \cos\frac{\sqrt{1-\mathrm{n}}}{\rho_0}(\mathrm{s}-\mathrm{s}_0) + \mathrm{x}'_0\frac{\rho_0}{\sqrt{1-\mathrm{n}}}\sin\frac{\sqrt{1-\mathrm{n}}}{\rho_0}(\mathrm{s}-\mathrm{s}_0) \\ \mathrm{y(s)} =& \mathrm{y}_0 \cos\frac{\sqrt{\mathrm{n}}}{\rho_0}(\mathrm{s}-\mathrm{s}_0) + \mathrm{y}'_0\frac{\rho_0}{\sqrt{\mathrm{n}}}\sin\frac{\sqrt{\mathrm{n}}}{\rho_0}(\mathrm{s}-\mathrm{s}_0) \end{aligned} \tag{1.11}$$

• Exercise 1.2.3-1. Plot the trajectory coordinates over 2-3 turns in the cyclotron, verify that they coincide with the expressions in Eq. 1.11. Give the analytical expression of the trajectory angles, $x'(s)$ and $y'(s)$. Plot and check. •

Note that the dissymmetry between the conditions of horizontal stability ($\mathrm{n} < 1$ and the "1" term in "$\sqrt{1-\mathrm{n}}$") and vertical stability ($0 < \mathrm{n}$) arises from the focusing introduced by the curvature, this is a purely geometrical effect. The associated focal distance to the curvature of a magnet of arc length $\mathcal{L}$ is obtained by integrating $\frac{\mathrm{d}^2\mathrm{x}}{\mathrm{ds}^2} + \frac{1}{\rho_0^2}\mathrm{x} = 0$ and identifying with the focusing property $\Delta x' = -x/f$, namely,

$$\Delta\mathrm{x}' = \int \frac{\mathrm{d}^2\mathrm{x}}{\mathrm{ds}^2}\mathrm{ds} \approx \frac{-\mathrm{x}}{\rho^2}\int \mathrm{ds} = \frac{-\mathrm{x}\mathcal{L}}{\rho^2}, \quad \text{thus} \quad \mathrm{f} = \frac{\rho^2}{\mathcal{L}}$$

Chromatism, chromatic orbit - In an axially symmetric structure, the equilibrium trajectory at momentum $\begin{cases}\mathrm{p}_0\\ \mathrm{p}_\mathrm{A}\end{cases}$ is at radius $\begin{cases}\rho_0 \text{ such that } \mathrm{B}_0\rho_0 = \mathrm{p}_0/\mathrm{q}\\ \rho_\mathrm{A} \text{ such that } \mathrm{B}_\mathrm{A}\rho_\mathrm{A} = \mathrm{p}_\mathrm{A}/\mathrm{q}\end{cases}$, with $\mathrm{B}_\mathrm{A} = \mathrm{B}_0 + \left(\frac{\partial \mathrm{B}}{\partial \mathrm{x}}\right)_0 + \ ...\ \rho_\mathrm{A} = \rho_0 + \Delta\mathrm{x}$, $\mathrm{p}_\mathrm{A} = \mathrm{p}_0 + \Delta\mathrm{p}$,

$$\mathrm{B}_\mathrm{A}\rho_\mathrm{A} = \frac{\mathrm{p}_\mathrm{A}}{\mathrm{q}} \Rightarrow \left[\mathrm{B}_0 + \left(\frac{\partial\mathrm{B}}{\partial\mathrm{x}}\right)_0 \Delta\mathrm{x} + ...\right][\rho_0 + \Delta\mathrm{x}] = \frac{\mathrm{p}_0 + \Delta\mathrm{p}}{\mathrm{q}} = \frac{\mathrm{p}_0}{\mathrm{q}} + \frac{\Delta\mathrm{p}}{\mathrm{q}}$$

and, neglecting terms in $(\Delta\mathrm{x})^2$: $\mathrm{B}_0\rho_0 + \left(\frac{\partial\mathrm{B}}{\partial\mathrm{x}}\right)_0\rho_0\Delta\mathrm{x} + \mathrm{B}_0\Delta\mathrm{x} = \frac{\mathrm{p}_0}{\mathrm{q}} + \frac{\Delta\mathrm{p}}{\mathrm{q}}$, which, given that $\mathrm{B}_0\rho_0 = \frac{\mathrm{p}_0}{\mathrm{q}}$, leaves $\Delta\mathrm{x}\left[\frac{\partial\mathrm{B}}{\partial\mathrm{x}}\rho_0 + \mathrm{B}_0\right] = \frac{\Delta\mathrm{p}}{\mathrm{q}}$, which given $\mathrm{n} = -\frac{\rho_0}{\mathrm{B}_0}\left(\frac{\partial\mathrm{B}}{\partial\mathrm{x}}\right)_0$ yields

$$\Delta\mathrm{x} = \frac{\rho_0}{1-\mathrm{n}}\frac{\Delta\mathrm{p}}{\mathrm{p}_0} = \mathrm{D}\frac{\Delta\mathrm{p}}{\mathrm{p}_0} \tag{1.12}$$

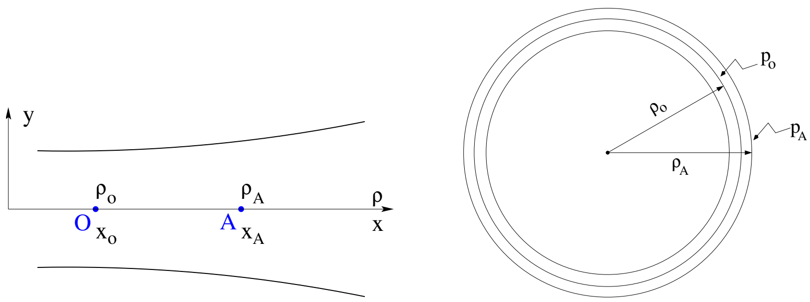

Fig. 1.8 Equilibrium radius is at $\rho = \rho_0$, $\mathrm{x} = \mathrm{x}_0$ for the particle with momentum p_0, rigidity $\mathrm{B}\rho = \mathrm{B}_0\rho_0$. Equilibrium radius is at $\rho = \rho_\mathrm{A}$, $\mathrm{x} = \mathrm{x}_\mathrm{A}$ for the particle with momentum $\mathrm{p}_\mathrm{A} = \mathrm{p}_0 + \Delta\mathrm{p}$, rigidity $\mathrm{B}\rho = \mathrm{B}_\mathrm{A}\rho_\mathrm{A}$.

where we introduce in passing the quantity $\mathrm{D} = \frac{\rho_0}{1-\mathrm{n}}$, the "dispersion" factor with respect to the reference closed orbit at ρ_0. This establishes that D(s) is the solution of the differential equation

$$\frac{\mathrm{d}^2\mathrm{D}}{\mathrm{ds}^2} + \frac{1-\mathrm{n}}{\rho_0^2}\mathrm{D} = \frac{1}{\rho_0} \tag{1.13}$$

and is a constant in the present case of the cylindrical-symmetry cyclotron structure.

Momentum compaction - A chromatic closed orbit $x(s) = D\frac{\Delta p}{p}$ has a different length, $\mathcal{L}+\delta\mathcal{L}$, with $\mathcal{L}$ the length of the "on-momentum" closed orbit. The trajectory lengthening, or "momentum compaction" compaction, is

$$\alpha = \frac{\Delta\mathcal{L}/\mathcal{L}}{\Delta\mathrm{p}/\mathrm{p}} = \frac{\Delta\mathrm{R}/\mathrm{R}}{\Delta\mathrm{p}/\mathrm{p}} = \frac{1}{(1-\mathrm{n})} = \frac{1}{\nu_\mathrm{x}^2} \tag{1.14}$$

with the rightmost expression by virtue of Eq. 1.8.

• Exercise 1.2.3-2. In the optical conditions of Ex, 1.2.3-1,
- check the trajectory lengthening of "chromatic orbits", Eq. 1.14 , plot it as a function of $\Delta p/p$,
- plot the dispersion term around the ring D(s), check that it does not depend on s,
- based on Fourier analysis of particle motion, check $\alpha = \frac{1}{\nu_\mathrm{x}^2}$, Eq. 1.14. •

Betatron wavelength - Introducing $\theta = \mathrm{s}/\rho$ as the independent variable Eq. 1.10 becomes

$$\frac{\mathrm{d}^2\mathrm{z}}{\mathrm{d}\theta^2} + \nu^2\mathrm{z} = 0, \quad \begin{cases} \text{radial motion}: \quad \mathrm{z} = \mathrm{x} \text{ and } \nu = \nu_\mathrm{x} = \sqrt{1-\mathrm{n}} \\ \text{vertical motion}: \mathrm{z} = \mathrm{y} \text{ and } \nu = \nu_\mathrm{y} = \sqrt{\mathrm{n}} \end{cases} \tag{1.15}$$

Both have the same form, that of the differential equation of the harmonic oscillator, with solution

$$\mathrm{z} = \mathrm{z}_0 \cos\nu\theta + \frac{\mathrm{z}_0'}{\nu}\sin\nu\theta, \quad \frac{\mathrm{dz}}{\mathrm{d}\theta} = -\nu\mathrm{z}_0\sin\nu\theta + \mathrm{z}_0'\cos\nu\theta \tag{1.16}$$

This can be written in the alternate form

$$\mathrm{z} = \hat{\mathrm{z}}\cos(\nu\theta+\phi), \quad \frac{\mathrm{dz}}{\mathrm{d}\theta} = -\nu\hat{\mathrm{z}}\sin(\nu\theta+\phi) \tag{1.17}$$

where,

$$\hat{\mathrm{z}} = \sqrt{\mathrm{y}_0^2 + \frac{\mathrm{y}_0'^2}{\nu^2}}, \quad \phi = -\mathrm{atan}\frac{\mathrm{y}_0'}{\nu\mathrm{y}_0} \tag{1.18}$$

The consequence is: $\hat{z}^2 = y_0^2 + \frac{y_0'^2}{\nu^2} = y^2 + \frac{y'^2}{\nu^2}$: $\hat{z}$ is an invariant of the motion.

• Exercise 1.2.4-1. Track a particle with small amplitude radial and axial motions, at constant energy, in a ring cyclotron based on the earlier material.
(i) Plot $\mathrm{x}(\theta)$, $\mathrm{y}(\theta)$ around the ring over 3-4 turns. Check that the observed fraction of wavelength per turn (radial or axial), identifies with the wave number (hint: use a fitting procedure to match the trajectory with the expected Eq 1.11). Check against theoretical expectation.
(ii) Record particle coordinates x, y at some s, compute its radial and axial wave numbers by Fourier analysis of its turn-by-turn coordinates x and y. What is the indetermination on the wave number?
(iii) At some azimuth s of the ring, observe the particle coordinates as it circles around, plot them (in both cases $\mathrm{z}=\mathrm{x}$, $\mathrm{z}=\mathrm{y}$) in a $(\mathrm{z}, \frac{1}{\nu_\mathrm{z}}\frac{\mathrm{dz}}{\mathrm{d}\theta})$ diagram. What is the form the the trajectory in that representation? In what direction, clockwise or counterclockwise, is the particle moving in that space? •

1.2.4 *Resonant acceleration*

An oscillating radio-frequency (RF) electric field, with fixed-frequency $\mathrm{f_{RF}} = \mathrm{f_{rev}}$ (harmonic h=1 of the revolution frequency), is applied in the gap between the two dees (Fig. 1.3). An ion of charge q reaching the gap at time t undergoes a change in energy

$$\Delta\mathrm{W}(\mathrm{t}) = \hat{\mathrm{V}}\sin\phi \quad \text{with } \phi = \omega_{\mathrm{RF}}\mathrm{t} - (\omega_{\mathrm{rev}}\mathrm{t} + \phi_0) \tag{1.19}$$

with ϕ the RF phase experienced by the particle at the time it crosses the gap and ϕ_0 the origin in phase for the particle motion (normally about $\pi/2$, at the crest of V(t) oscillation). Note that this ignores the "transit time", the effect of the time that the particle spends across the gap on the overall energy gain; focusing in the cyclotron as well, in what follows, will ignore the effect of the electric gap.

The frequency dependence of the kinetic energy W of the ion relates to its orbital radius R in the following way:

$$W = \frac{1}{2}mv^2 = \frac{1}{2}m(2\pi Rf_{rev})^2 = \frac{1}{2}m(2\pi R\frac{f_{RF}}{h})^2 \tag{1.20}$$

thus, for a given cyclotron size (R), f_{RF} and h set the limit for the acceleration range.

The revolution time/frequency increases/decreases with energy and the condition of synchronism between the revolution time of the ion and the oscillating voltage, $f_{RF} = hf_{rev}$, is only fulfilled at one particular radius in the course of acceleration (Fig. 1.9). To the left and to the right, outphasing $\Delta\phi$ builds-up turn after turn, decreasing in a first stage (towards zero and lower voltages, Fig. 1.9-right) and then increasing (back to the starting $\phi = \pi/2$ phase and beyond towards $V < 0$, deceleration).

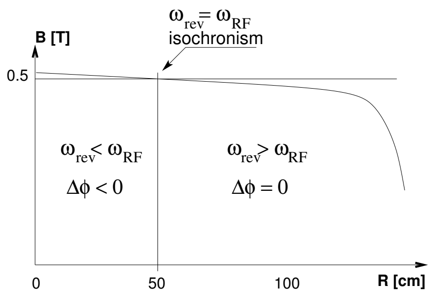

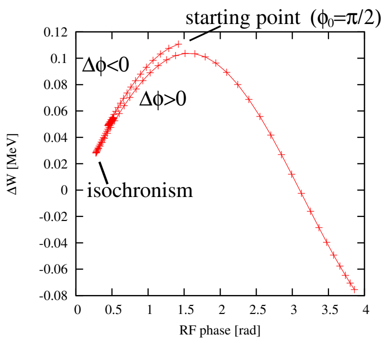

Fig. 1.9 Synchronous condition at one point (left), and span in phase of the accelerating voltage in $[0^o, 180^o]$ range (left).

Differentiating the phase, $\dot{\phi} = \omega_{RF} - \omega_{rev}$ (Eq. 1.19), and considering that over a turn $\Delta\phi = \dot{\phi}\frac{\pi R}{v}$, one gets

$$\Delta\phi = \pi\left(\frac{m\omega_{RF}}{qB} - 1\right) \tag{1.21}$$

Due to this cumulative outphasing the classical cyclotron requires quick acceleration (limited number of turns), which means high voltage (tens of kVolts). As expected, with ω_{RF} and B constant, $\Delta\phi$ presents a minimum

($\dot{\phi} = 0$) at $\omega_{\rm RF} = \omega_{\rm rev} = \frac{\rm qB}{\rm m}$ where exact isochronism is reached (Fig. 1.9). The upper limit to ϕ is set by the condition $\Delta{\rm W} > 0$, acceleration.

• Exercise 1.2.4-1. In a cyclotron based on the earlier material, install a double gap as in Fig. 1.3, with a peak gap voltage $\hat{\rm V} = 100$ kV. Set the voltage frequency such that acceleration is independent of the arrival phase. Track a proton from 1 to 5 MeV. Plot the path length and revolution period as a function of energy, compare that accelerated orbit with the "static" one in ex. 1.2.1-1. Plot the evolution of its phase at the gap along with the voltage in a V(t) diagram, as in Fig. 1.9-right. •

• Exercise 1.2.4-2. In the conditions of exercise 1.2.4-1, set the voltage frequency equal to the revolution frequency at R=50 cm (this is about half-way to the desired extraction radius at 5 MeV). Check the energy-phase equation of the cyclotron,

$$\cos\phi - \cos\phi_0 = \pi\left[1 - \frac{\omega_{\rm RF}}{\omega_{\rm rev,in}}(1 + \frac{\rm W}{2{\rm m_0c^2}})\right]\frac{\rm W}{{\rm q}\hat{\rm V}} \quad \bullet \tag{1.22}$$

1.3 Relativistic cyclotron

The bad news with relativistic energies, is, from the cyclotron resonance $\omega_0 = {\rm qB}/\gamma{\rm m_0}$, given ${\rm R} = \beta{\rm c}/\omega_0$, one gets

$${\rm k} = \frac{\rm R}{\rm B}\frac{\partial{\rm B}}{\partial{\rm R}} = \frac{\beta}{\gamma}\frac{\partial\gamma}{\partial\beta} = \beta^2\gamma^2 \tag{1.23}$$

Thus k is positive and increases with energy: the weak focussing condition $-1 < {\rm k} < 0$ is not satisfied.

• Exercise 1.3-1. In passing, demonstrate (or correct in case of an error) the following relationships:
$\frac{\rm dp}{\rm p} = \frac{1}{\beta^2}\frac{\rm dE}{\rm E}$; $\frac{d\beta}{\beta} = \frac{1}{\gamma^2}\frac{\rm dp}{\rm p} = \frac{1}{\beta^2\gamma^2}\frac{\rm dE}{\rm E}$; $\frac{d\gamma}{\gamma} = \frac{\rm dW}{\rm m_0+W}$ (W = kinetic energy); $\frac{\rm dW}{\rm W} = \frac{\gamma+1}{\gamma}\frac{\rm dp}{\rm p}$. •

The revolution period on the equilibrium orbit, momentum p = qBR and circumference $\mathcal{C}$, is ${\rm T} = \mathcal{C}/\beta{\rm c} = 2\pi\gamma{\rm m_0}/{\rm qB}$. Isochronism requires p-invariant revolution period, dT/dp = 0. Differentiating the previous expression, this requirement yields

$${\rm B(R)} = \frac{\rm B_0}{\gamma_0}\gamma({\rm R}) \tag{1.24}$$

with B_0 and γ_0 free reference conditions, and the reference revolution period is noted T_0. In other words, isochronism requires $B(R) \propto \gamma$, which happens to yield axial defocusing!

There was a paper by H.A. Bethe and M.E. Rose stressing, "... it seems useless to build cyclotrons of larger proportions than the existing ones... an accelerating chamber of 37 cm radius will suffice to produce deuterons of 11 MeV energy which is the highest possible...". Frank Cole : "If you went to graduate school in the 1940s, this inequality $[-1 < k < 0]$ was the end of the discussion of accelerator theory."

Until...

1.3.1 *Thomas focusing*

In 1938, L.H. Thomas introduces the concept of alternating regions of stronger and weaker axial field, the "AVF" (Azimuthally Varying Field) cyclotron. The single-magnet concept of the classical cyclotron remains, the azimuthal field modulation is obtained by shaping the magnet pole to create a $2\pi/N$-periodical field form factor, the "flutter" form factor, for instance of the form (Fig. 1.11)

$$\mathcal{F}(\theta) \propto 1 + f \sin(N\theta) \tag{1.25}$$

The radial increase of the field (Eq. 1.24) for isochronism of the orbits is obtained by radial pole shaping. The median plane field now varies with both R and θ,

$$B(R, \theta) = B_0\, \mathcal{R}(R)\, \mathcal{F}(\theta) \tag{1.26}$$

This azimuthal variation of the field amplitude introduces an azimuthal component in the field index :

$$k = \frac{\rho}{B}\frac{dB}{dx} = \frac{\rho}{B}\left[\frac{\partial B}{\partial R}\frac{dR}{dx} + \frac{\partial B}{\partial \theta}\frac{d\theta}{dx}\right] \tag{1.27}$$

Note the introduction of a local curvature radius, $\rho(s)$, as the orbit curvature is no longer constant along the orbit as a consequence of the AVF.

A sector dipole with index

We now introduce the transfer matrix of a sector magnet, pushing Thomas' modulation to the point that the field varies abruptly between 0 and B_0 at sector edges (a "hard-edge" sector). Bending sections span a fraction of 2π and the "filling factor" (ratio of magnetic length to circumference

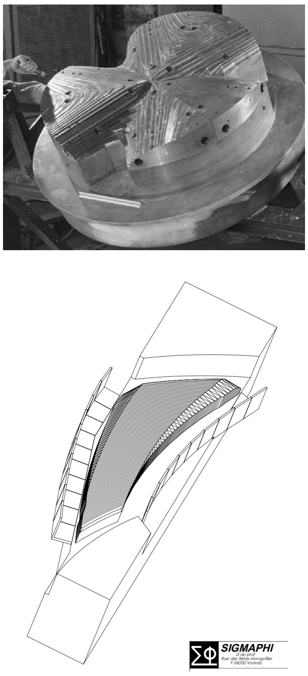

Fig. 1.10 Top: azimuthal pole shaping in Thomas-style AVF cyclotron. Bottom: the pole of a spiral sector dipole in a magnet computation code.

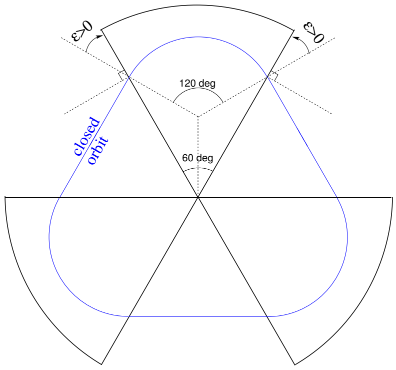

Fig. 1.11 Sketch of a separated sector cyclotron, based on 120 degree sectors. The actual magnet edges have a $\epsilon = 30$ degree "wedge angle" with respect to the 120 degree sector. This is a "closing" of the magnet, is causes vertical focusing and weakens the horizontal focusing compared to a 120 degree wedge magnet (*cf.* Fig. 1.13).

along a closed orbit, $\mathrm{L_{mag}}/2\pi\mathrm{R}$) is < 1. Coordinate transport through the hard-edge bending sector writes (just another way of expressing Eq. 1.11)

$$\begin{pmatrix} \mathrm{x} \\ \mathrm{x}' \\ \mathrm{y} \\ \mathrm{y}' \end{pmatrix}_{\mathrm{out}} = \begin{pmatrix} \cos\sqrt{k_x}\mathcal{L} & \frac{1}{\sqrt{k_x}}\sin\sqrt{k_x}\mathcal{L} & 0 & 0 \\ -\sqrt{k_x}\sin\sqrt{k_x}\mathcal{L} & \cos\sqrt{k_x}\mathcal{L} & 0 & 0 \\ 0 & 0 & \cos\sqrt{k_y}\mathcal{L} & \frac{1}{\sqrt{k_y}}\sin\sqrt{k_y}\mathcal{L} \\ 0 & 0 & -\sqrt{k_y}\sin\sqrt{k_y}\mathcal{L} & \cos\sqrt{k_y}\mathcal{L} \end{pmatrix} \begin{pmatrix} \mathrm{x} \\ \mathrm{x}' \\ \mathrm{y} \\ \mathrm{y}' \end{pmatrix}_{\mathrm{in}} \tag{1.28}$$

wherein $\mathrm{k_x} = (1-\mathrm{n})/\rho^2$, $\mathrm{k_y} = \mathrm{n}/\rho^2$, $\mathcal{L}$ is the length of the arc of curvature ρ (which coincides with the trajectory of reference momentum $\mathrm{p} = \mathrm{mv}$ at radius R).

• Exercise 1.3.1-1. Compute the 4×4 transport matrix of a 60^{o} sector with index $0 < \mathrm{n} < 1$ (say, $\mathrm{n} = 0.6$) and curvature ρ for the reference momentum p (Fig. 1.12-left), from the ray-tracing of an appropriate set of rays. Compare with theory. •

• Exercise 1.3.1-2. The focal distance associated with the curvature (index

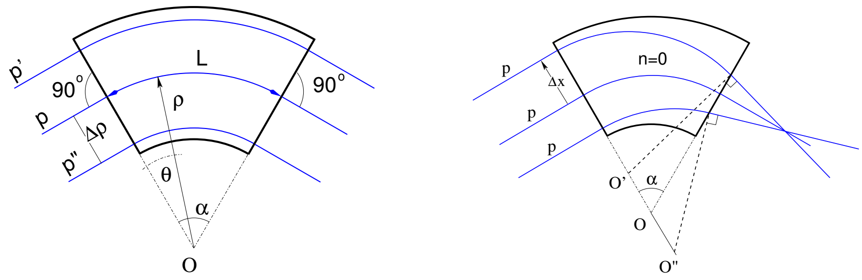

Fig. 1.12 Left: an $\alpha = 60^o$ sector dipole with index n. At constant radius, B is constant, a particle with *small* momentum deviation $\Delta p = q(1-n)B\Delta\rho$ will follow an arc of radius $\rho + \Delta\rho$. Right, case of field index n = 0: parallel incoming rays of equal momenta come out converging. Convergence of a uniform field sector dipole is a geometrical property.

n = 0, magnet length $\mathcal{L}$ and curvature radius ρ) satisfies
$$\frac{\mathrm{d^2x}}{\mathrm{ds^2}} + \frac{1}{\rho^2}\mathrm{x} = 0 \Rightarrow \Delta\mathrm{x}' = \int \frac{\mathrm{d^2x}}{\mathrm{ds^2}}\mathrm{ds} \approx -\frac{\mathrm{x}}{\rho^2}\int \mathrm{ds} = -\frac{\mathrm{x}}{\rho^2}\mathcal{L} \stackrel{\mathrm{def.}}{\equiv} -\frac{\mathrm{x}}{\mathrm{f}} \Rightarrow \mathrm{f} = \frac{\rho^2}{\mathcal{L}}$$
Verify the value of f for paraxial rays with incidence zero and incoming coordinates ±x. •

• Exercise 1.3.1-3. Cancelling the geometrical focusing effect of a constant field dipole (Fig. 1.12-right) requires particles at greater (smaller) radius to find a smaller (greater) field. It would result in ΔB such that $\Delta\mathrm{x} = \mathrm{OO}' = 0$. Differentiation of $\mathrm{B}\rho = \mathrm{C^{st}}$ yields $\frac{\Delta \mathrm{B}}{\mathrm{B}} + \frac{\Delta\rho}{\rho}$, thus a required index $\mathrm{n} = -\frac{\rho}{\mathrm{B}}\frac{\Delta\mathrm{B}}{\Delta\mathrm{x}} = 1$. Verify that by ray-tracing parallel incoming rays of equal momenta. •

Wedge focusing

A note in passing: wedge focusing would eventually be the technique used for the ZGS, “Zero Gradient Synchrotron”, a 12 GeV ring at Argonne. This will be addressed in the weak focusing synchrotron chapter. It simplifies the sector magnet as it avoids profiling its poles (as $n = 0$).

The transport of the transverse (radial and axial) particle coordinates through a dipole magnet edge, with wedge angle ϵ can be written under the matrix form
$$\begin{pmatrix} x \\ x' \\ y \\ y' \end{pmatrix}_2 \begin{pmatrix} 1 & 0 & 0 & 0 \\ -\tan\frac{\epsilon}{\rho} & 1 & 0 & 0 \\ 0 & 0 & 1 & 0 \\ 0 & 0 & \tan\frac{\epsilon}{\rho} & 1 \end{pmatrix} \begin{pmatrix} x \\ x' \\ y \\ y' \end{pmatrix}_1 \qquad (1.29)$$

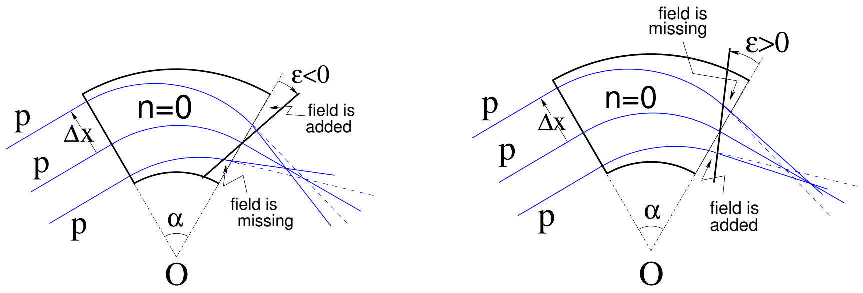

Fig. 1.13 Left: a focusing wedge, opening the sector augments the horizontal focusing. Right: a defocusing wedge, closing the sector diminishes the horizontal focusing. Focal distance in the bend plane respectively decreases, increases. The reverse holds in the vertical plane, opening/closing the sector decreases/increases the vertical focusing.

The transport matrix through a wedge magnet with identical wedge at both ends writes

$$\mathrm{M} = \mathrm{W_o} \times \mathrm{M_{sector}} \times \mathrm{W_i} \tag{1.30}$$

with $\mathrm{W_o}$, exit wedge (respectively $\mathrm{W_i}$, entrance wedge) a matrix of the form Eq. 1.29 and M the sector matrix of Eq. 1.28.

• Exercise 1.3.1-6. From ray-tracing, get the transport matrix of a 120° sector in the two cases of (i) no wedge angle, (ii) 30° wedge angle at entrance and exit as sketched in Fig. 1.11. Show that in the second case the dipole is both radially and axially focusing. Check against Eq. 1.29 . •

The "flutter" F characterizes the steepness of the azimuthal field fall-off $\mathcal{F}(\theta)$ over an extent λ at magnet ends. For a given orbit, of average radius $\mathrm{R} = \oint \mathrm{ds}/2\pi$ and of curvature $\rho(\mathrm{s})$ inside the dipole, it writes

$$\mathrm{F} = \left(\frac{<\mathcal{F}^2> - <\mathcal{F}>^2}{<\mathcal{F}>^2}\right)^{1/2} \xrightarrow{\lambda\to 0} \frac{\mathrm{R}}{\rho} - 1 \tag{1.31}$$

with $\mathrm{F} = \mathrm{fracR}\rho - 1$ the "hard-edge" field fall-off case, *i.e.*, the (unphysical) case when $\mathcal{F}(\theta)$ steps from 1 to 0 at the location of the magnet edge. Edge focussing allows the necessary $\mathrm{B(R)} \propto \gamma(\mathrm{R})$ (Eq. 1.24) by the ensuring axial focusing. If the scalloping of the orbit is small, *i.e.*, if $\mathcal{C}/2\pi \approx \rho$ (*i.e.*, the presence of drifts only causes a small departure of the $\mathcal{C}$-circumference closed orbit from the average radius $\mathcal{C}/2\pi$))

$$\nu_\mathrm{x} \approx \sqrt{1-\mathrm{n}} \quad \text{and} \quad \nu_\mathrm{y} \approx \sqrt{\mathrm{n}+\mathrm{F}^2} \tag{1.32}$$

in a first approach. The flutter causes $\mathrm{n}+\mathrm{F}^2 > 0$ (whereas $\mathrm{n} < 0$, B increases with R for isochronism) thus the vertical motion is stable in the sense of periodic stability (ν_y real). Expectedly from what precedes, the fringe field modifies the first order vertical mapping, namely, the wedge focussing (Eq. 1.29) is changed in the following way:

$$\mathrm{R}_{43=}\frac{\tan(\epsilon)}{\rho} \to \mathrm{R}_{43} = \frac{\tan(\epsilon-\psi)}{\rho} \tag{1.33}$$

wherein

$$\psi = \mathrm{I}_1 \frac{\lambda}{\rho}\frac{1+\sin^2\epsilon}{\cos\epsilon}, \quad \text{with } \mathrm{I}_1 = \int_{\mathrm{s}|_{\mathrm{B}=0}}^{\mathrm{s}|_{\mathrm{B}=\mathrm{B}_0}} \frac{\mathrm{B(s)}(\mathrm{B}_0-\mathrm{B(s)})}{\mathrm{B}_0^2}\frac{\mathrm{ds}}{\lambda} \tag{1.34}$$

with $B(s)$ the median-plane field, ϵ the wedge angle (Fig. 1.13), and the integral I_1 extends over the field fall-off where B evolves in the range $[0, B_0]$, B_0 being the field value reached inside the magnet. Horizontal focusing is only affected to second order in the $(\mathrm{x}, \mathrm{x}')$ coordinates, the first order mapping of Eq. 1.29 is unchanged.

• Exercise 1.3.1-7. Play with the extent λ of the fringe field in the 120 degree sector magnet of Ex. 1.3.1-5: from extremely short (quasi hard-edge) to very long. Check the evolution of horizontal and vertical focusing of the magnet, and of the wave numbers in the ring cyclotron. •

1.3.2 *Spiral sector*

In 1954 Kerst introduces a method for vertical wedge focusing which compensates for the radially increasing field gradient: by spiraling the edges of the sector dipoles (Figs. 1.1 , 1.10-bottom)

$$\mathrm{B}(\mathrm{R},\theta) = \mathrm{B}_0\,\mathcal{F}(\mathrm{R},\theta)\,\mathcal{R}(\mathrm{R}), \quad \mathcal{F}(\mathrm{R},\theta) = 1+\mathrm{f}\sin(\mathrm{N}(\theta-\tan(\xi)\ln(\mathrm{R}/\mathrm{R}_0)))) \tag{1.35}$$

$R = R_0\exp(\theta/\tan(\xi))$ is the equation of the spiral, centered at the center of the ring. This results in a larger contribution of the flutter term in the vertical wave number,

$$\nu_\mathrm{z} = \sqrt{\mathrm{n}+\mathrm{F}^2(1+2\tan^2\xi)} \tag{1.36}$$

with ξ the spiral angle: the angle that the tangent to the spiral edge does with the ring radius.

In the late 1950s appeared the "separated sector cyclotron", in which the the sector dipoles are separated by iron-free (but not really field-free) spaces (Fig. 1.2). Isochronous cyclotrons nowadays still rely on these various principles and techniques, their limit in energy resides in achievable field strength, magnet size, and beam separation at the last turn for extraction.

An instance of a single-magnet spiral sector AVF cyclotron is PSI's 250 MeV protontherapy machine, Fig. 1.1, the field at the center of the cyclotron is 2.4 T. An instance of a separated spiral sector cyclotron is PSI's 590 MeV, Fig. 1.2. Simulations regarding fixed-field spiral sector optics are postponed to the FFAG chapter.

1.3.3 *Isochronous acceleration*

Data regarding PSI cyclotron (Fig. 1.2) are provided in a separate document, co-authored by M. Haj Tahar (Columbia University) and F. Méot.

1.4 summary

During this laboratory work session, we have learned about the following:

- the uniform field (single-magnet) classical cyclotron, field characterized by B(θ) =constant, slowly decreasing with R for vertical stability of the motion,

- weak transverse focusing, in both planes simultaneously, defined by an hyperbolic radial dependence of the field, $B(R) = B_0 \frac{R_0}{R^\alpha} \quad (0 < \alpha < 1)$,

- near-crest loosely-isochronous resonant acceleration in the classical cyclotron,

- Thomas' isochronous single-magnet "AVF" cyclotron; azimuthal field modulation ("flutter") and vertical focusing, with for instance $B(\theta) \propto B_0(1 + f\sin(3\theta))$,

- wedge focusing, enhanced vertical wedge focusing by a spiraling the pole,

- the isochronous cyclotron, a separated sector ring accelerator,

- isochronous resonant acceleration in PSI cyclotron.

Various notions and quantities proper to the characterization of charged particle dynamics in accelerators have been introduced, including:

- closed orbit,

- field index, focusing,

- differential equations of the motion, and their periodic solutions,

- betatron wavelength, motion invariant,

- dispersion function,

- transport of particle coordinates, dipole and wedge transport matrices.

1.5 Appendix

1.5.1 *Optical sequence for Exercise 1.1-1 .*

The cyclotron is defined using a 360 degree field map. This optical sequence can be copy-pasted to a Zgoubi input data file and run as it is, once the magnetic field map has een built (and saved in “geneSectorMap.out“).

```
Uniform field sector
 'OBJET'
64.62444403717985                        ! 200keV proton
2
1 1
12.9248888074 0.  0.   0.   0.  1. 'm'
1
 'PARTICUL'   ! This is required only because we want to get the time-of-flight
PROTON       ! otherwise zgoubi only requires rigidity.

 'FAISTORE'
zgoubi.fai
1
 'TOSCA'
0  2
1.  1. 1. 1.
HEADER_8
315 121 1 22.1 1.        IZ=1 -> 2D ; MOD=22 -> polar map ; .MOD2=.1 -> one map file
geneSectorMap.out
0 0 0 0
2
1.
2
0. 0. 0. 0.
6
```

1.5.2 *Optical sequence for Exercise 1.2.1-1.c*

The cyclotron is defined using a mathematical model for the dipole field, a 60 degree sector. This optical sequence can be copy-pasted to a Zgoubi input data file and run as it is.

```
Cyclotron, classical.
 'OBJET'
64.62444403717985                                 ! 200keV
2
4 1
12.9248888074 0.  0.   0.   0.  1. 'm'             ! 200keV. R=Brho/B=*/.5
28.9070891209 0.  0.   0.   0.  2.23654451125 'm'   ! 1 MeV. R=Brho/B=*/.5
50.           0.  0.   0.   0.  3.86850523397 'o'   ! at RM  (B*rho=0.5*0.5=0.25T.m, 2.9885 MeV)
64.7070336799 0.  0.   0.   0.  5.0063899693  'M'   ! 5 MeV. R=Brho/B=*/.5
1 1 1 1

 'DIPOLE'
0
60. 50.
30.  5. 0. 0. 0.
0.  0.                                      ! EFB 1  hard-edge
4  .1455   2.2670  -.6395  1.1558  0. 0.  0.
30. 0.  1.E6  -1.E6  1.E6  1.E6
0.   0.                                     ! EFB 2
4  .1455   2.2670  -.6395  1.1558  0. 0.  0.
-30. 0.  1.E6  -1.E6  1.E6  1.E6
0. 0.                                       ! EFB 3
0  0.      0.      0.      0.      0. 0.  0.
0. 0.  1.E6  -1.E6  1.E6  1.E6 0.
4   10.
1.                  ! The smaller, the better the orbits close.
2  0. 0. 0. 0.       ! Could also be, e.g., 2 50. 0. 50. 0. with Y0 amended accordingly in OBJET
 'FAISCEAU'
 'FAISTORE'
 zgoubi.fai
 1
 'END'
```

Bibliography

E.O.Lawrence and N.E.Edlefsen, Science 72, 376 (1930);

E.O.Lawrence and M.S. Livingston, Phys. Rev. 37 (1931), 1707; 38, 136, (1931); 40, 19 (1932) H.A.Bethe and M.E.Rose, Phys. Rev. 54, 588 (1938)

L.H.Thomas, *The Paths of Ions in the Cyclotron*, Phys. Rev. 54, 580, (1938)

F. Chautard, *Beam Dynamics For Cyclotrons*, in *CERN Accelerator School*, Zeegse, The Netherlands, 24 May-2 June 2005.

J. Le Duff, *Longitudinal beam dynamics in circular accelerators*, in *CERN Accelerator School*, Jyvaskyla, Finland, 7-18 September 1992.

T. Stammbach, *Introduction to Cyclotrons*, in *CERN accelerator school, cyclotrons, linacs and their applications*, IBM International Education Centre, La Hulpe, Belgium, 28 April-5 May 1994.

H. A. Enge, Deflecting magnets, in Focusing of Charged Particles, Vol. 1, A. Septier Ed., Academic Press (1967).